Available online at www.sciencedirect.com

ScienceDirect

Procedia Structural Integrity 68 (2025) 465–471

Structural Integrity Procedia

www.elsevier.com/locate/procedia

European Conference on Fracture 2024

Comparative Study of Fatigue Behavior and Microstructural Evolution in As-Built and Heat-Treated Additively Manufactured 316L Stainless Steel

Atef Hamada[a,*], Matias Jaskari[a], Walaa Abd-Elaziem[b], Tarek Allam[c], Antti Järvenpää[a]

[a]*Future Manufacturing Technologies FMT, Kerttu Saalasti Institute, University of Oulu, Pajatie 5, 85500 Nivala, Finland*
[b]*Departmen of Materials Science and Engineering, Northwestern University, Evanston, IL 60208, United States Institute of Energy and Climate*
[c]*Research: Structure and Function of Materials (IEK-2), Forschungszentrum Jülich GmbH, 52425, Jülich, Germany*

Abstract

This study investigates the influence of heat treatment (HT) at 900 °C on the fatigue resistance of 316L stainless steel fabricated through selective laser melting (SLM). Fully reversed, force-controlled fatigue tests were conducted on both as-built (AB) and HTed specimens to assess their cyclic deformation behavior and fatigue life. The fatigue fracture mechanisms were analyzed through detailed microstructural characterization using secondary electron imaging in a scanning electron microscope (SEM) and laser scanning confocal microscope LSCM. Results show that the HT 316L exhibited improved fatigue resistance and a longer fatigue life compared to the AB 316L. Fatigue cracking along dendritic columnar grains and the formation of slip bands were identified as key microstructural features in both AB and HT materials. In the AB material, the columnar dendritic grains and cellular substructure appear to create weak points at grain boundaries, facilitating fatigue crack initiation due to localized strain in persistent slip bands. However, HT at 900 °C effectively reduced the cellular substructure, promoting the formation of high-angle grain boundaries, which significantly enhanced the fatigue resistance of HT 316L.

Keywords: Laser-powder bed fusion ; 316L stainless steel ; heat treatment ; microstructure ; fatigue fracture

* Corresponding author.
E-mail address: atef.hamadasaleh@oulu.fi

10.1016/j.prostr.2025.06.083

1. Introduction

Recent publications and review articles on additive manufacturing (AM) technology for metallic materials highlight its potential to revolutionize various industrial sectors, including aerospace, medical, automotive, and general manufacturing. AM enables the production of complex designs that are difficult or cost-prohibitive to create using traditional manufacturing methods (du Plessis et al., 2022; Hamza et al., 2022). However, a significant concern regarding metallic materials fabricated by AM is their fatigue performance, which is critical for their acceptance in structural applications subjected to cyclic loading, a common cause of mechanical failure in many engineering structures (Yadollahi and Shamsaei, 2017). The processing parameters of AM can significantly influence the microstructure, as well as the presence of internal and surface defects, ultimately affecting the mechanical properties of the materials (Abd-Elaziem et al., 2022). Among these materials, 316L stainless steel is widely used across various industrial applications, such as in the medical, chemical, marine, nuclear, and aerospace sectors(Lo et al., 2009). Its popularity is attributed to its excellent thermal stability, high corrosion resistance, and favorable mechanical properties at both room and cryogenic temperatures. Consequently, numerous studies have focused on the mechanical properties and fatigue resistance of AM 316L.

For instance, (Becker et al., 2021) provided a comprehensive review of the HCF strength of AM 316L fabricated using laser-powder bed fusion (L-PBF) under both as-built (AB) and post-processing conditions. Their findings indicated a low fatigue resistance in AB 316L, with an HCFS of just 90 MPa. Pelegatti et al. (2022) investigated the key factors contributing to low cycle fatigue in LB-PBF 316L, emphasizing that premature crack nucleation often arises from surface voids. They also noted that defects resulting from lack of fusion, particularly those exceeding 400 μm in size, are more detrimental to fatigue life than smaller semi-spherical pores. Liang et al. (2022) conducted high cycle fatigue (HCF) tests on both AB and hand-polished AM 316L under various loading modes (tension, bending, and torsion) and found that inherent surface defects significantly degrade fatigue performance. In the same context, (Hatami et al., 2020) examined the effects of post-machining on the HCF of AB 316L at a stress ratio of R = 0.1, reporting that post-machined specimens exhibited higher fatigue strength compared to their AB counterparts due to reduced pore and surface defect presence. (Pegues et al., 2020) studied the mechanical properties and fatigue performance of LB-PBF 304L stainless steel after post-machining and electro-polishing, concluding that the unique microstructural features of LB-PBF 304L enhance its fatigue resistance compared to its wrought equivalent by mitigating typical fatigue crack initiation mechanisms, such as annealing twin boundaries (Σ3-TB) and high-angle grain boundaries (HAGB).

This study contributes to the existing literature by systematically investigating the effects of heat treatment (HT) at 900 °C on the fatigue behavior of AM 316L stainless steel. While previous research has primarily focused on AB and post-processed conditions, this work uniquely explores how HT alters the microstructural characteristics and enhances fatigue resistance in AM 316L. By employing a comprehensive approach that combines force-controlled fatigue testing with advanced microstructural characterization techniques, this study aims to elucidate the specific deformation and damage mechanisms at play in the HCF regime

2. Experimental procedures

The 316L powder used in this study was supplied by Electro Optical Systems Oy (EOS) and was sieved to eliminate larger particles exceeding 50 μm. The chemical composition of the powder is presented in Table 1. Fatigue specimen blanks, which were round with a total length of 54 mm, a gauge length of 12 mm, and a minimum diameter of 6 mm, were vertically 3D-printed by LB-PBF technique in (EOS, Turku, Finland). The LB-PBF process employed an incremental layer thickness of 80 μm and industrial parameters to achieve a volumetric energy density (VED) of 40 J/mm³. Layers were successively added until the full structure height was completed. The AB 316L specimens underwent HT at 900 °C for 30 minutes in a muffle furnace (Nether) under an argon atmosphere.

HCF tests were conducted at room temperature using a Zwick electromagnetic resonator fatigue machine (Vibrophore) with a maximum load of 50 kN, following a symmetrical push-pull cycle in force control mode. The tests were performed at a frequency of 100 Hz with zero mean stress. The fatigue damage mechanisms were investigated by examining the microstructures of the fatigued specimens using a laser scanning confocal microscope (LSCM) (Model: KEYENCE/VK-X200). The fracture surfaces of the cyclically fatigued materials, both AB and HT 316L, were

analyzed through secondary electron SEM imaging in a field emission gun scanning electron microscope (FEG-SEM; Carl Zeiss Ultra plus).

Table 1: Chemical composition of the 316L powder supplied for L-PBF manufacturing, along with the corresponding composition of the AB material.

Element, wt.%	C	Mn	Cr	Ni	Mo	Cu	Si
powder	0.03	2	17/19	13/15	2.2/3	0.5	0.75
AB	0.018	1.42	17.9	12.8	3	0.24	0.34

3. Results and discussion

The microstructures of the AB and HT 316L, as observed using LSCM, are shown in Fig. 1. In the AB 316L, Fig. 1(a), typical features associated with L-PBF are evident, including the characteristic "fish scale morphology" and well-defined melt pool boundaries. A dendritic structure with columnar grains and a cellular substructure is also visible. These microstructural characteristics align with those reported in previous studies on L-PBF manufactured 316L (Edin et al., 2022; Qiu et al., 2018; Yan et al., 2018). The cellular substructure, formed due to rapid solidification, features high-density dislocation networks and elemental segregation along the cell boundaries, as described by (Sun et al., 2016). The microstructure of the 316L after annealing at 900 °C is shown in Fig. 1(b). While the material retains some of the features of the AB microstructure, significant changes are evident. Notably, high-angle grain boundaries become more prominent due to the breakdown of the dendritic substructure at 900 °C (Fig. 1b), although a small fraction of the columnar grains remains. This observation is consistent with findings by Edin et al., (2022) who reported that the cellular structure of AB 316L begins to break down at 800 °C and is largely eliminated at 900 °C.

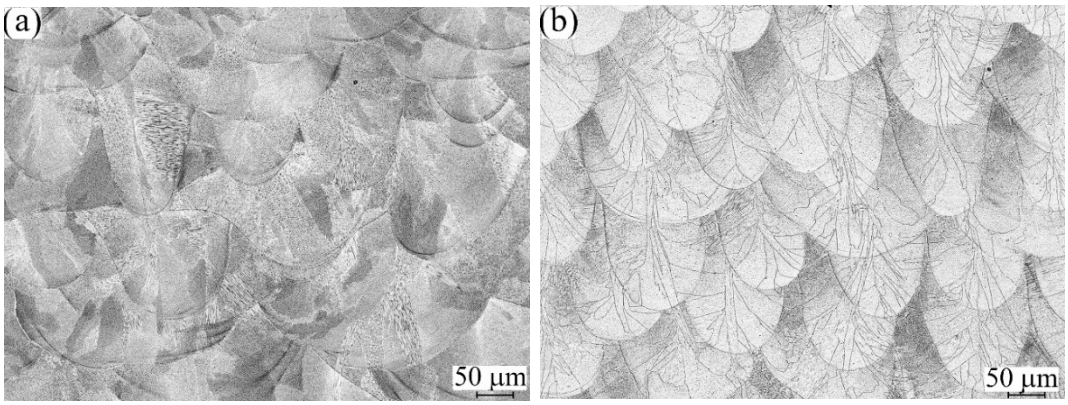

Fig.1: Laser scanning confocal microscope images of L-PBF manufactured 316L : (a) as-built (AB) condition, and (b) microstructure after HT at 900 °C for 30 min.

The HCF behavior of the AM 316L stainless steel was evaluated up to 10^7 cycles using a high-efficiency electromagnetic resonance fatigue testing machine. Figure 2 presents the S-N curve (stress amplitude vs. number of cycles to failure) for both the AB and HT 316L samples. For reference, recent HCF data from Subasic et al. (2024) and Maleki et al. (2024) are included for comparison. It is important to note that the printing parameters and VEDs used in their studies, 53 J/mm³ and 76.4 J/mm³, respectively—differ from the VED of 40 J/mm³ used in this work, which affects the resulting microstructure and mechanical properties of the 316L. A significant improvement in fatigue resistance is observed for the HT 316L. The AB 316L exhibited a relatively low HCF strength of approximately 75 MPa, typical of AM materials due to the presence of inherent microstructural defects like porosity, lack of fusion, and surface irregularities. These defects act as stress concentrators, promoting early crack initiation and reducing fatigue life. After HT at 900°C, the HCF strength of the 316L increased to approximately 150 MPa, indicating a substantial enhancement in fatigue performance. This improvement is attributed to the elimination of the cellular substructure

and the development of high-angle grain boundaries, which increase the resistance to crack initiation and propagation during cyclic loading.

Comparing the results to the literature, the 316L printed with EOS parameters in the current study shows superior fatigue resistance. Subasic et al. (2024) reported an S-N curve for AB 316L fabricated by L-PBF, but with a notably lower fatigue resistance. The fatigue lives reported by Subasic et al. were significantly lower at corresponding stress levels, with a fatigue limit of only 65 MPa, compared to the 75 MPa for the AB 316L in this study. This difference can be linked to the variations in printing parameters and energy densities, which directly impact the microstructure and defect distribution. The results indicate that the EOS-printed material in the current work outperforms the material studied by Subasic et al., in terms of both fatigue strength and life. Table 2 shows that the 316L material printed using the EOS machine, even with a lower VED, demonstrates superior fatigue strength compared to other studies, regardless of fatigue test parameters such as loading type, stress ratio, and frequency.

Dastgerdi et al. (2022) reported S-N plots for AM 316L fabricated by L-PBF with vertical and horizontal build orientations and layer thicknesses of 20 µm and 40 µm. They found that build orientation and layer thickness significantly affect fatigue resistance, with vertically built samples generally outperforming horizontally built ones. However, the AB 316L materials did not exhibit a distinct fatigue limit, likely due to internal and surface defects. In contrast, the current study's 316L materials, both AB and HT, displayed clear fatigue limits of 75 MPa and 150 MPa, respectively. This underscores the effectiveness of HT in reducing microstructural defects and enhancing fatigue life. Wang et al. (2021) also compared the fatigue performance of AM 316L with its wrought counterpart. They reported that L-PBF manufactured 316L exhibited a lower fatigue limit (90 MPa) compared to wrought 316L (166.5 MPa), primarily due to residual stresses and anisotropic grain structures in the AM material. The present study's HT 316L, with its fatigue limit of 150 MPa, approaches the performance of wrought material, demonstrating the value of HT in bridging the gap between AM and conventionally manufactured materials. These results show that HT at 900°C significantly enhances the fatigue resistance of L-PBF-manufactured 316L stainless steel. The improvement in HCF strength from 75 MPa to 150 MPa highlights the critical role of post-processing in mitigating defects and optimizing the mechanical performance of AM materials. These findings contribute to the growing understanding of how post-processing can bring AM 316L closer to meeting the stringent demands of HCF applications, making it a more viable option for structural components subjected to cyclic loading.

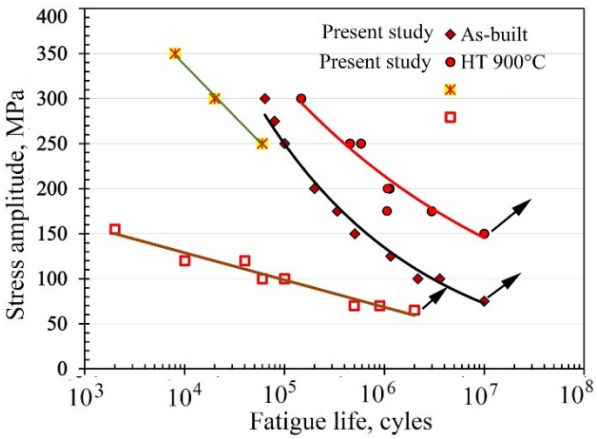

Figure 2: Stress amplitude–fatigue life (S–N) curves for high-cycle fatigue testing of AM 316L in both as-built and HT conditions. Comparative data from literature for 316L printed using selective laser melting (SLM) at various volumetric energy densities (VEDs) are included for reference.

Table 2: Comparison between the fatigue strength of AM 316L (as-built) related to the AM machine and VED printing

	AM Machine	VED J/mm^3	fatigue loading	stress ratio R	Hz	Fatig. limit
Present study	EOS	40	axial	-1	100	75
Maleki et al., (2024)	SLM	76.4	bending	-1	10	N/A
Subasic et al., (2024)	Renishaw	53	uniaxial	0.1	20	65

The fracture surfaces of the fatigued AB and HT 316L were examined using SE imaging. Figure 3 presents the key features observed on the fracture surfaces of the AB specimen fatigued at a stress amplitude of 100 MPa. In Figure 3(a), a lack-of-fusion (LOF) defect associated with the presence of oxides, indicated by an arrow, is visible. This internal defect acts as a stress concentrator, leading to crack initiation under cyclic loading. Such LOF defects are typical of AM materials, where incomplete melting of adjacent powder layers can cause internal voids or flaws. In another location, Figure 3(b) highlights subsurface defects, including a semi-spherical pore with a diameter of 35 µm (marked by a yellow circle) and a LOF defect with diagonal dimensions of 68 µm and 80 µm (indicated by a red pentagon). These defects disrupt the continuity of the microstructure, creating regions of localized stress concentration. Under dynamic cyclic loading, these defects experience localized plastic deformation, leading to microcrack formation at the defect sites, as also noted by Hamada et al. (2023). Figure 3(c) reveals slip traces on multiple facets of the fracture surface. These slip lines are believed to be the result of persistent slip bands (PSBs) forming during cyclic deformation, which intersect the fracture surface. The presence of PSBs is an indication of localized cyclic plasticity, where dislocations accumulate, weakening the material and leading to crack initiation and propagation. As depicted in Figure 3(d), quasi-cleavage fracture features, accompanied by secondary cracks, are clearly observable. The grain boundaries in the AB microstructure serve as preferential sites for crack initiation and propagation, particularly under HCF conditions. This behavior is driven by the combined effects of stress concentration at microstructural defects and the intrinsic weaknesses of the grain boundary regions. Consequently, the dendritic structure facilitates quasi-cleavage fracture, accelerating crack propagation during cyclic loading.

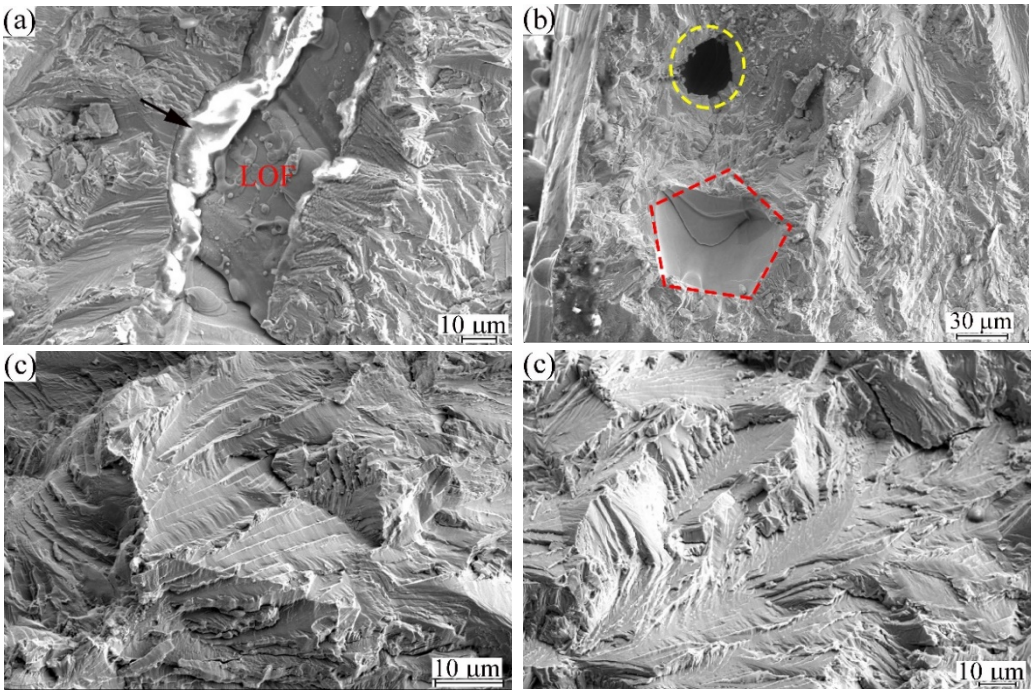

Fig. 3. SEM images of the fracture surface of the fatigued AB 316L at the stress amplitude of 150 MPa: (a) Lack-of-Fusion and oxide defects, (b) large void and LOF, (c) persistent slip bands (PSBs), (d) semi-cleavage fracture

Fig. 4 presents the fracture surface features of HTed 316L subjected to cyclic loading at a stress amplitude of 200 MPa. It is evident from Fig. 4(a) that fatigue crack initiation occurs primarily at the interfaces of surface-adhered particles, highlighted by the red arrows. These surface particles, likely remnants of the L-PBF process, create local stress concentrations, which serve as preferential sites for crack initiation under cyclic loading. The presence of these particles, despite HT, suggests that surface finish and particle adhesion remain critical factors affecting fatigue performance. In Fig. 4(b), the fracture surface exhibits densely clustered fatigue slip bands without observable defects. These fatigue markings, which form as a result of cyclic plastic deformation, indicate that the material underwent extensive localized strain during fatigue loading. The presence of PSBs is a characteristic of fatigue deformation in FCC metals. As the cyclic strain progresses, PSBs intersect the grain boundaries, similar to what is commonly seen in fatigued polycrystalline FCC metals (Man et al., 2009). These intersections can act as sites for fatigue crack embryos, ultimately leading to the initiation of microcracks. The intense formation of PSBs in the HT 316L, as observed in this study, suggests that the HT promoted more uniform deformation mechanisms and a reduction in defect-driven crack initiation. Fig. 4(c) highlights a large LOF defect associated with oxides, which still exists in the HT specimen. Despite the stress relief provided by the HT, this LOF defect remains a site of high local stress concentration and serves as a point of fatigue crack initiation. The LOF defect, resulting from incomplete melting during the L-PBF process, typically features sharp geometries that exacerbate stress localization, making it a critical factor in fatigue failure. Similarly, Fig. 4(d) shows a round pore associated with oxides, another type of manufacturing defect that contributes to fatigue cracking. Pores act as voids where stress concentrates, accelerating crack initiation and propagation. These defects, both LOF and pores, are inherent to the AM process and significantly influence the fatigue life of the material. Despite the presence of these defects, it is apparent that HT at 900°C for 30 min, functioning as a stress-relief (SR) process, significantly reduces their detrimental effects. This thermal treatment alleviates intrinsic tensile residual stresses that are typically introduced during the rapid solidification of the AM process. Residual stresses, if not relieved, can significantly promote crack initiation and propagation by creating regions of high localized stress. HT also helps in homogenizing the microstructure and reducing internal stresses, thereby enhancing the fatigue resistance of the material. Thus, the HT 316L exhibits improved fatigue behavior compared to the AB condition. By reducing the influence of internal defects and mitigating residual stresses. This emphasizes the importance of post-processing treatments in optimizing the mechanical performance of AM components.

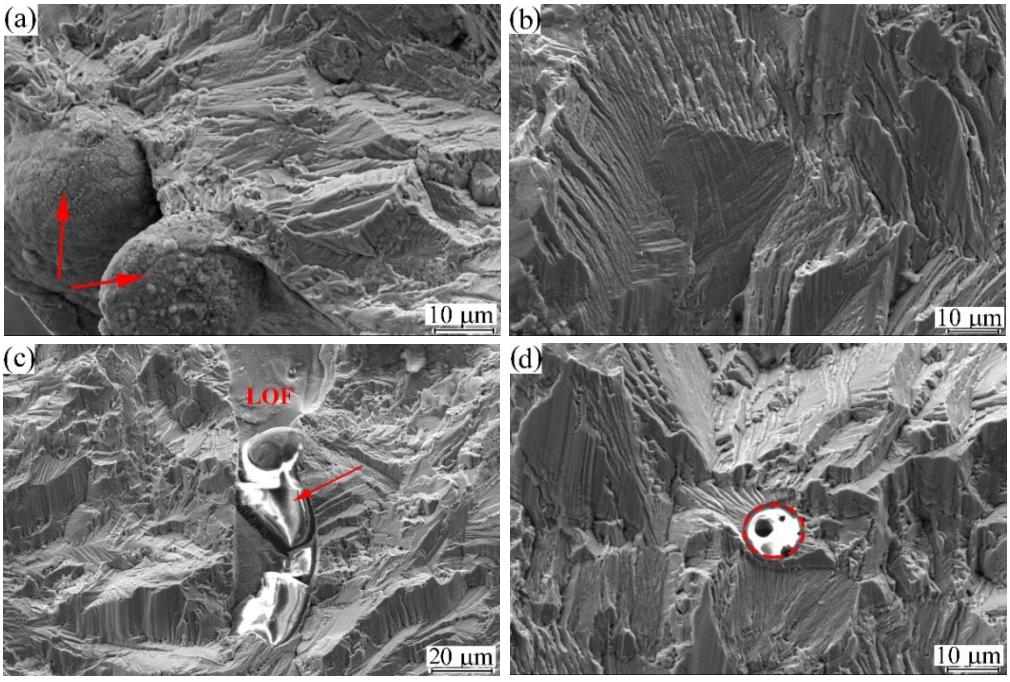

Fig. 4. SEM images of the fracture surface of the fatigued HT 316L at the stress amplitude of 200 MPa: (a) fatigue crack site at the surface particles adhered to the outer surface , (b) initiation site related to unfused surface particles, (b) intensive persistent slip bands (PSBs) on the fracture surface, (c) Lack-of-Fusion and oxide defects withing the matrix, and (d) fatigue crack initiation related to internal pore

4. Conclusions

1.The fatigue strength of AB 316L stainless steel manufactured using L-PBF showed a substantial improvement after HT at 900°C. The fatigue limit increased from 75 MPa in the AB condition to 150 MPa after HT. This enhancement is attributed to the reduction in residual stresses and the breakdown of the cellular microstructure, both of which contribute to the material's increased resistance to cyclic loading.
2.In the AB condition, fatigue damage in AM 316L is primarily driven by L-PBF-induced defects such as pores, dendritic cellular structures, and residual stresses. These microstructural features act as stress concentrators, leading to crack initiation and propagation. HT at 900°C significantly mitigated these effects, reducing the influence of these defects and promoting more uniform fatigue behavior.

References

Abd-Elaziem, W., Elkatatny, S., Abd-Elaziem, A.E., Khedr, M., Abd El-Baky, M.A., Hassan, M.A., Abu-Okail, M., Mohammed, M., Järvenpää, A., Allam, T., Hamada, A., 2022. On the current research progress of metallic materials fabricated by laser powder bed fusion process: a review. J. Mater. Res. Technol. 20, 681–707. https://doi.org/10.1016/J.JMRT.2022.07.085

Becker, T.H., Kumar, P., Ramamurty, U., 2021. Fracture and fatigue in additively manufactured metals. Acta Mater. 219, 117240. https://doi.org/10.1016/J.ACTAMAT.2021.117240

du Plessis, A., Razavi, N., Benedetti, M., Murchio, S., Leary, M., Watson, M., Bhate, D., Berto, F., 2022. Properties and applications of additively manufactured metallic cellular materials: A review. Prog. Mater. Sci. 125, 100918. https://doi.org/10.1016/J.PMATSCI.2021.100918

Edin, E., Svahn, F., Åkerfeldt, P., Eriksson, M., Antti, M.L., 2022. Rapid method for comparative studies on stress relief heat treatment of additively manufactured 316L. Mater. Sci. Eng. A 847, 143313. https://doi.org/10.1016/J.MSEA.2022.143313

Hamada, A., Jaskari, M., Gundgire, T., Järvenpää, A., 2023. Enhancement and underlying fatigue mechanisms of laser powder bed fusion additive-manufactured 316L stainless steel. Mater. Sci. Eng. A 873, 145021. https://doi.org/10.1016/J.MSEA.2023.145021

Hamza, H.M., Deen, K.M., Khaliq, A., Asselin, E., Haider, W., 2022. Microstructural, corrosion and mechanical properties of additively manufactured alloys: a review. Crit. Rev. Solid State Mater. Sci. 47, 46–98. https://doi.org/10.1080/10408436.2021.1886044

Hatami, S., Ma, T., Vuoristo, T., Bertilsson, J., Lyckfeldt, O., 2020. Fatigue Strength of 316 L Stainless Steel Manufactured by Selective Laser Melting. J. Mater. Eng. Perform. 29, 3183–3194. https://doi.org/10.1007/S11665-020-04859-X/FIGURES/16

Liang, X., Hor, A., Robert, C., Salem, M., Lin, F., Morel, F., 2022. High cycle fatigue behavior of 316L steel fabricated by laser powder bed fusion: Effects of surface defect and loading mode. Int. J. Fatigue 160, 106843. https://doi.org/10.1016/J.IJFATIGUE.2022.106843

Lo, K.H., Shek, C.H., Lai, J.K.L., 2009. Recent developments in stainless steels. Mater. Sci. Eng. R Reports 65, 39–104. https://doi.org/10.1016/J.MSER.2009.03.001

Maleki, E., Unal, O., Doubrava, M., Pantelejev, L., Bagherifard, S., Guagliano, M., 2024. Application of impact-based and laser-based severe plastic deformation methods on additively manufactured 316L: Microstructure, tensile and fatigue behaviors. Mater. Sci. Eng. A 147360. https://doi.org/10.1016/J.MSEA.2024.147360

Man, J., Obrtlík, K., Polák, J., 2009. Extrusions and intrusions in fatigued metals. Part 1. State of the art and history†. Philos. Mag. 89, 1295–1336. https://doi.org/10.1080/14786430902917616

Nafar Dastgerdi, J., Jaberi, O., Remes, H., 2022. Influence of internal and surface defects on the fatigue performance of additively manufactured stainless steel 316L. Int. J. Fatigue 163, 107025. https://doi.org/10.1016/J.IJFATIGUE.2022.107025

Pegues, J.W., Roach, M.D., Shamsaei, N., 2020. Additive manufacturing of fatigue resistant austenitic stainless steels by understanding process-structure–property relationships. Mater. Res. Lett. 8, 8–15. https://doi.org/10.1080/21663831.2019.1678202

Pelegatti, M., Benasciutti, D., De Bona, F., Lanzutti, A., Magnan, M., Srnec Novak, J., Salvati, E., Sordetti, F., Sortino, M., Totis, G., Vaglio, E., 2022. On the factors influencing the elastoplastic cyclic response and low cycle fatigue failure of AISI 316L steel produced by laser-powder bed fusion. Int. J. Fatigue 165, 107224. https://doi.org/10.1016/J.IJFATIGUE.2022.107224

Qiu, C., Kindi, M. Al, Aladawi, A.S., Hatmi, I. Al, 2018. A comprehensive study on microstructure and tensile behaviour of a selectively laser melted stainless steel. Sci. Reports 2018 81 8, 1–16. https://doi.org/10.1038/s41598-018-26136-7

Subasic, M., Olsson, M., Dadbakhsh, S., Zhao, X., Krakhmalev, P., Mansour, R., 2024. Fatigue strength improvement of additively manufactured 316L stainless steel with high porosity through preloading. Int. J. Fatigue 180, 108077. https://doi.org/10.1016/J.IJFATIGUE.2023.108077

Sun, Z., Tan, X., Tor, S.B., Yeong, W.Y., 2016. Selective laser melting of stainless steel 316L with low porosity and high build rates. Mater. Des. 104, 197–204. https://doi.org/10.1016/J.MATDES.2016.05.035

Wang, Z., Yang, S., Huang, Y., Fan, C., Peng, Z., Gao, Z., 2021. Microstructure and Fatigue Damage of 316L Stainless Steel Manufactured by Selective Laser Melting (SLM). Mater. 2021, Vol. 14, Page 7544 14, 7544. https://doi.org/10.3390/MA14247544

Yadollahi, A., Shamsaei, N., 2017. Additive manufacturing of fatigue resistant materials: Challenges and opportunities. Int. J. Fatigue 98, 14–31. https://doi.org/10.1016/J.IJFATIGUE.2017.01.001

Yan, F., Xiong, W., Faierson, E., Olson, G.B., 2018. Characterization of nano-scale oxides in austenitic stainless steel processed by powder bed fusion. Scr. Mater. 155, 104–108. https://doi.org/10.1016/J.SCRIPTAMAT.2018.06.011